# A Three-Dimensional Finite Element Analysis of a Two-Axially Pre-Loaded Plate Exposed to a Dynamic Force

Ahmet DASDEMIR* iD

*Kastamonu University, Faculty of Science, Department of Mathematics, Kastamonu, Türkiye*

<u>**Highlights**</u>
• 3D forced vibration analysis of an elastic plate with initial stress is given.
• Effect of various polarization directions on resonances of system is investigated.
• Dynamical modeling of the problem and its FEM are created.

| Article Info | Abstract |
|---|---|
| | In this paper, the forced vibration analysis by a harmonically time-dependent force of an elastic plate covered rigidly by a rigid half-plane is given. The plate layer is subjected to bi-axial normal initial force, into lateral sides separately. Here, the preloading state is exactly static and homogeneous. To eliminate the disadvantage of such a nonlinear model, the problem formulation is modeled in terms of the fundamental consideration of the theory of linearized wave in elastic solids under a pre-loaded state (TLWESPS) in a plane-stress case. For this purpose, considering Hamilton's principles, the system of the partial equations of motion and the boundary-contact conditions are found. Based on the virtual work and the fundamental theorem of the calculus of variation, the three-dimensional finite element method (3D-FEM) is used to understand the dynamic behavior of the plate. A numerical validation process is established based on error norm functions. Next, influences of certain problem parameters such as Young's modulus, aspect ratio, thickness ratio, pre-loaded parameter, etc. on the frequency mode of the pre-stressed system are given. The numerical investigations show that higher values of Poisson's ratio promote the resonant mode of the plate while increasing the influence of the preloaded parameter on the dynamic response of the plate. |
| | |

## 1. INTRODUCTION

A body is called elastic material if returning to its reference shape upon the removal of the applied forces. In fact, all the materials exhibit elastic behavior for sufficient small forces. It is well-known that mathematical investigations of the elastic response of a body constitute the theory of elasticity. The interdependence between the force of the system and the resultant stresses/deformations has been an important topic in several practical applications for a long time. The books by Barber [1] and Lurie [2] noted detailed information related to this topic.

According to the open literature, the idea of modeling an interrelationship between the elastic force and deformation was put forward for the first time by the famous English scientist Robert Hooke in 1678. Nevertheless, a general mathematical consideration of the elasticity of theory was not created until the nineteenth century. After a development process that started with Navier's investigation of the general field equations and that continued with Cauchy's investigation of basic elasticity relations and the concept of stress, the theory of elasticity took shape with a long list of prominent scientists and mathematicians such as Bernoullis, Kelvin, Poisson, Lamé, Kirchhoff, Rayleigh, Love, Timoshenko, and so on.

*e-mail: ahmetdasdemir37@gmail.com

Within the scope of the theory of elasticity, investigating relevant wave propagation problems in an elastic medium is very difficult due to many factors like material properties, the configuration of the problem, etc. A nonlinear state may appear in the problem. Therefore, to be able to make it possible to obtain the solution, certain theoretical attempts were done. At the beginning of the 20th century, the first important venture was done by Southwell [3], laying down the foundation of a new theoretical approach, which is termed "Three-Dimensional Linearized Equations (TDLE)". The theory eliminates the nonlinear wave propagation issue in the medium. However, as mentioned above, additional problem conditions increase the degree of nonlinearity of the problem. Therefore, this theory must be adapted to new cases. Due to the mentioned reasons, Biezeno and Henky contributed to the adaptation process of TDLE [4]. To find a solution to different types of problems, TDLE has been updated under certain assumptions by several scientists, i.e., Biot [5], Neuber [6], Trefftz [7], and Green et al. [8], Guz [9], Zubov [10], Tiersten [11], Ogden [12], Akbarov and Guz [13], and Reddy [14].

In the 1950s, the importance of results related to the dynamic behavior of initially stressed (or pre-loaded) mediums was realized by mechanic scientists. However, the initial stress concept yields the nonlinear stress waves in the medium. Based on certain assumptions, the general nonlinear case can be linearized or simplified. This allows for the investigation of dynamic problems for pre-loaded bodies. In particular, there are two different approaches for identifying the assumptions, i.e., (i) approximate approach and (ii) exact approach. The first one is based on the reduction of dimension under the Bernoulli, Kirchhoff–Love, and Timoshenko hypotheses; namely, in this case, three-dimensional problems turn into two-dimensional ones and two-dimensional ones to one-dimensional ones. To be clear, although the approximate approaches ease the solution process, the results can be meaningless, both qualitatively and quantitatively. For example, the near-surface dynamic behavior of the pre-loaded medium cannot be analyzed. Hence, the exact approach may be the most appropriate preference and is termed the theory of linearized wave in elastic solids under a pre-loaded state (TLWESPS). It should be stated that the fundamental principles of TLWESPS were created by Guz [15]. By the way, the investigations of TLWESPS can also be classified into two groups. While the papers in the first group investigate wave propagations, the ones in the second group deal with stress distributions in the medium. Akbarov presented a wide investigation related to this theory and its modifications [16].

Due to applications of the concept of "initial stress" or "pre-load", there are many papers in the open literature. Here, a brief survey is presented for TLWESPS. Kepçeler studied torsional wave dispersion through the imperfect interface of an elastic bi-layered cylinder that is initially stressed into a thickness direction [17]. Zamanov and Agasiyev solved the Lamb-type problem in a pre-stressed system involving three-layered compressible elastic materials with infinite horizontal lengths [18]. Eröz presented a vibration analysis for a pre-loaded elastic plate subjected to a timely harmonic loading, standing on a rigid half-plane [19]. Akbarov et al. investigated the influence of incomplete contact interaction on the dynamic behavior of the two-layered plate with pre-load under a perpendicular dynamic force [20]. Hu et al. derived dispersion relations for axisymmetric waves in a circular cylindrical pipe that is initially stressed into a lateral surface [21]. Ilhan and Koç reported their results on the effect of poling direction on wave propagation in a piezoelectric slab standing on a piezoelectric half-plane [22]. Kurt et al. analyzed near-surface wave propagation in a pre-stressed elastic strip resting on a pre-loaded piezoelectric half-plane [23]. Yeşil solved forced and natural vibration problems of a pre-loaded three-dimensional orthotropic slab involving two neighboring cylindrical cavities [24]. Daşdemir modeled the dynamic behavior of a pre-loaded piezoelectric strip with finite length exposed to a harmonic force resting on a rigid half plane [25]. Daşdemir simulated finite element analysis of a system of two pre-loaded elastic layers with finite lengths subjected to a point-wise dynamic force, standing on a rigid ground [26]. Selim derived the dispersion relationship of TWs in a pre-loaded single-walled carbon nanotube with surface irregularity within the scope of Flügge shell theory [27]. Babych and Glukhov investigated the effect of a moving force on the dynamic response of a pre-loaded compounded plate [28]. Mandi et al. studied torsional wave propagation in a pre-loaded stratified structure with transversely isotropic, porous layer, inhomogeneous medium, and visco-elastic semi-infinite medium [29]. Bagirov considered the mechanical problem in the axisymmetric waves propagating by the contacting of the longitudinal cuts in a cylinder [30]. Kumawat et al. discussed the torsional wave in a pre-loaded compounded cylinder made of imperfectly bonded Steel, Aluminum, and Bronze [31]. Daşdemir analyzed the dynamic response of a pre-loaded piezoelectric slab that can be

polarized in various axial directions and that is under a harmonic force [32]. Veliyev and Ipek investigated the dispersion of axisymmetric quasi-Scholte waves in the initially nonhomogeneous loaded hollow cylinder including an intrinsic compressible inviscid fluid [33]. Dehghanian et al. analyzed wave propagation analysis of pre-loaded incompressible hyperelastic multi-layered plates in terms of the first-order shear deformation plate theory [34].

In [35], Daşdemir and Eröz started a discussion to be able to understand the dynamic reaction of a three-dimensional slab with pre-loads under a perpendicular force, based on a rigid half-plane. However, the mentioned paper contains a limited investigation of the problem under consideration. For this reason, it would be important to search for a further numerical investigation related to a finite dimensional pre-stressed elastic system, i.e., in particular, to highlight the frequency response of the problem. A detailed mathematical model is created and the equations of motion are presented, in addition to boundary-contact terms. In the context of the virtual work principle and the calculus of variation, a three-dimensional finite element model is established for solving the resultant problem. Following, the outcomes of the paper are presented for the effects of Young's modulus, thickness ratio, aspect ratio, and initial stress parameter on the problem.

The current study is split into sub-sections to present the content as clear guidance as follows. Section 2 displays the structure of the problem, including partial differential equations and the respective boundary-contact terms, while section 3 models the solution procedure. The first part of section 4 gives the validation of the presented model while the rest part displays the numerical results. Finally, the important findings are encapsulated in the conclusion part.

## 2. PROBLEM FORMULATION

A three-dimensional elastic plate, whose architecture can be observed in Figure 1, with the dimension of $2a \times 2b \times h$ is considered in the current paper. According to the geometrical configuration, the volume and outward surfaces of the plate are denoted by $D$ and $S$. To be clear, they are defined as follows:

$$D = \left\{ \left( x_1, x_2, x_3 \right) : 0 \leq x_1 \leq 2a, \ -h \leq x_2 \leq 0, \ 0 \leq x_3 \leq 2b \right\} \tag{1}$$

$$S = S_1 \big|_{x_1=2a} \bigcup S_2 \big|_{x_3=2b} \bigcup S_3 \big|_{x_1=0} \bigcup S_4 \big|_{x_3=0} \bigcup S_5 \big|_{x_2=0} \bigcup S_6 \big|_{x_2=-h} \tag{2}$$

where $x_i$ is the Cartesian coordinate component, which coincides with the Lagrangian coordinate component $x_i'$. It should be noted that the origin point is located to the left-front corner of the free surface.
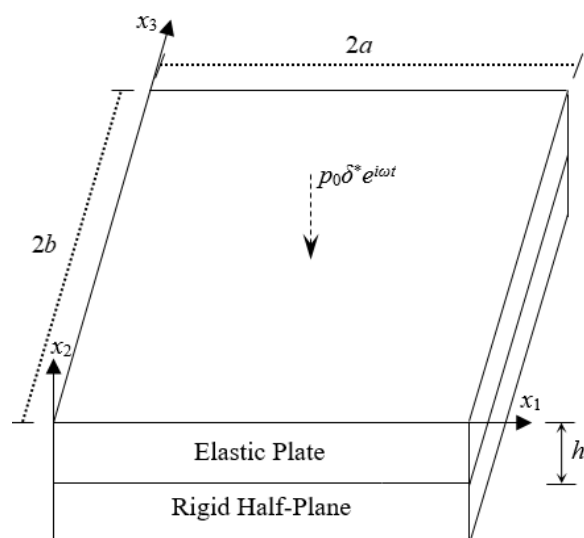


***Figure 1.*** *Geometry of the problem*

The production of the plate can be summarized as follows. First, the plate is made of isotropic, homogeneous, and moderately elastic materials in the shape of a rectangular prism. The resultant body is caused by a normal force in a horizontal direction, and then the same process is repeated for other horizontal direction. This yields a pre-load case in the medium. Note that the applied force may be whether tension or compression. On the other hand, there are two assumptions for this process: (i) the normal forces are strictly static and homogeneous, and (ii) the amplitudes of the dynamic perturbations are considerably smaller than those of the pre-deformations. In this case, our investigation can be conducted with TLWESPS, eliminating nonlinearity, and thus, the initial stress case can be defined as follows:

$$\sigma_{11}^{\;0} = q_{11}, \;\; \sigma_{33}^{\;0} = q_{33}, \text{ and } \sigma_{ij}^{\;0} = q_{ij} \text{ for otherwise} \tag{3}$$

where $q_{11}$ and $q_{33}$ are a constant, the top index "0" represents the pre-load case, and $i, j = 1, 2, 3$.

Following this, the plate is put forward to a rigid half-plane and then is affected by a dynamic force with a harmonic variable of time $t$ with frequency $\omega$ such that $e^{i\omega t}$. In this case, all the problem functions, i.e., displacement, strain, and stress components, can be clarified to harmonic and amplitude parts. In addition, we can utilize a transformation rule to study the problem in normalized coordinates, namely $\bar{x}_i = x_i / h$. For simplicity, we neglect the upper dashes and overbars. As a result, the equations of motion are given as follows [15]:

$$\sigma_{ij,j} + q_{kj} u_{i,jk} + \rho h^2 \omega^2 u_i = 0 \tag{4}$$

where $\sigma_{ij}$ and $u_i$ are stress and displacement components, $\rho$ is the mass density, the subscripts after a comma denote the coordinate derivative, and repeated indices imply the conventional summation rule. In addition, the strain-displacement relation between the stresses and strains can be defined as

$$\mathbf{S} = \mathbf{CE} \text{ and } \mathbf{S} = \mathbf{LU} \tag{5}$$

where

$$\mathbf{S} = \{\sigma_{11} \;\; \sigma_{22} \;\; \sigma_{33} \;\; \sigma_{23} \;\; \sigma_{13} \;\; \sigma_{12}\}^T, \; \mathbf{E} = \{\varepsilon_{11} \;\; \varepsilon_{22} \;\; \varepsilon_{33} \;\; 2\varepsilon_{23} \;\; 2\varepsilon_{13} \;\; 2\varepsilon_{12}\}^T, \; \mathbf{U} = \{u_1 \;\; u_2 \;\; u_3\}^T$$

$$\mathbf{C} = \frac{E}{1+\nu} \begin{bmatrix} \dfrac{1-\nu}{1-2\nu} & \dfrac{\nu}{1-2\nu} & \dfrac{\nu}{1-2\nu} & 0 & 0 & 0 \\[2mm] \dfrac{\nu}{1-2\nu} & \dfrac{1-\nu}{1-2\nu} & \dfrac{\nu}{1-2\nu} & 0 & 0 & 0 \\[2mm] \dfrac{\nu}{1-2\nu} & \dfrac{\nu}{1-2\nu} & \dfrac{1-\nu}{1-2\nu} & 0 & 0 & 0 \\[2mm] 0 & 0 & 0 & \dfrac{1}{2} & 0 & 0 \\[2mm] 0 & 0 & 0 & 0 & \dfrac{1}{2} & 0 \\[2mm] 0 & 0 & 0 & 0 & 0 & \dfrac{1}{2} \end{bmatrix} \text{ and } \mathbf{L} = \begin{bmatrix} \dfrac{\partial}{\partial x_1} & 0 & 0 & 0 & \dfrac{\partial}{\partial x_3} & \dfrac{\partial}{\partial x_2} \\[2mm] 0 & \dfrac{\partial}{\partial x_2} & 0 & \dfrac{\partial}{\partial x_3} & 0 & \dfrac{\partial}{\partial x_1} \\[2mm] 0 & 0 & \dfrac{\partial}{\partial x_3} & \dfrac{\partial}{\partial x_2} & \dfrac{\partial}{\partial x_1} & 0 \end{bmatrix}^T$$

where $E$ is the Young's modulus, $\nu$ is the Poisson's ratio, $\varepsilon_{ij}$ is the strain component, and the letter "$T$" denotes transpose operator.

The boundary-contact conditions for the current situation are follows:

I. Dynamic force conditions

$$\left.\sigma_{21}\right|_{x_2=0} = 0, \ \left.\sigma_{22}\right|_{x_2=0} = -p_o\delta^*, \ \left.\sigma_{23}\right|_{x_2=0} = 0,$$  (6)

II. Robin boundary conditions at the lateral sides

$$\left.\left(\sigma_{i1} + q_{11}u_{i,1}\right)\right|_{x_1=0,2a} = 0, \ \left.\left(\sigma_{i3} + q_{33}u_{i,3}\right)\right|_{x_3=0,2b} = 0$$  (7)

III. Rigid foundation conditions

$$\left.u_i\right|_{x_2=-1}$$  (8)

where $p_0$ is the amplitude of the external loading and $\delta^*$ is the Dirac's delta-function such that $\delta^* = \delta\left(\{x_1 - a\}^2 + \{x_3 - b\}^2\right)$.

## 3. FINITE ELEMENT PROCEDURE

In this section, a solution method to the problem is developed by employing the finite element method since the plate under consideration has finite lengths in each axial direction. However, it should be noted that a big data can be obtained due to the nature of the method. To do this, we first construct a weak form for the current analysis. Let us consider the virtual displacement function $\mathbf{V}$ that satisfies the same identities with the principal displacement vector $\mathbf{U}$. If multiplying the system of equations in Equation (4) with the virtual displacement function and integrating all the resultant statements over the problem volume, we obtain

$$0 = \int_D\left[\mathbf{V}^T\left(\mathbf{S}+\mathbf{S}^0\mathbf{E}\right)_{,j} + \rho\omega^2h^2\mathbf{V}^T\mathbf{U}\right]dD = \int_D\left[\left(\mathbf{V}^T\mathbf{S}+\mathbf{V}^T\mathbf{S}^0\mathbf{E}\right)_{,j} - \mathbf{E}_v^{\ T}\left(\mathbf{S}+\mathbf{S}^0\mathbf{E}\right)\right]dD + \rho\omega^2h^2\int_D\mathbf{V}^T\mathbf{U}dD \quad (9)$$

where the subscript "$v$" denotes terms related to the virtual functions. Next, using the famous Ostrogradsky theorem yields

$$\rho\omega^2h^2\int_D\mathbf{V}^T\mathbf{U}dD - \int_D\left[\mathbf{E}_v^{\ T}\left(\mathbf{S}+\mathbf{S}^0\mathbf{E}\right)\right]dD = \int_S\left[\left(\mathbf{V}^T\mathbf{S}+\mathbf{V}^T\mathbf{S}^0\mathbf{E}\right)\cos\left(\mathbf{n},x_j\right)\right]dS$$  (10)

where $\mathbf{n}$ is the unit normalized vector and $\cos\left(\mathbf{n},x_i\right)$ is the direction cosine. Considering the surfaces of the volume in Equation (2) and the boundary-contact terms in Equations (6)-(8), we get

$$\rho\omega^2h^2\int_D\mathbf{V}^T\mathbf{U}dD - \int_D\left[\mathbf{E}_v^{\ T}\left(\mathbf{S}+\mathbf{S}^0\mathbf{E}\right)\right]dD - \int_{S_5}\mathbf{V}^T\mathbf{f}dS_5 = 0$$  (11)

where $\mathbf{f}$ is the force. Equation (11) is the weak form of our problem. According to Hamilton's principle and the virtual work principle [36], we can write

$$0 = \rho\omega^2h^2\int_D\delta\mathbf{U}^T\mathbf{U}dV - \int_D\left[\delta\mathbf{E}^T\left(\mathbf{S}+\mathbf{S}^0\mathbf{E}\right)\right]dD - \int_{S_5}\delta\mathbf{U}^T\mathbf{f}dS_5$$

and from Equation (5),

$$0 = \rho \omega^2 h^2 \int_D \delta \mathbf{U}^T \mathbf{U} dV - \int_D \left[ \delta \mathbf{E}^T \left( \mathbf{C} + \mathbf{S}^0 \right) \mathbf{E} \right] dD - \int_{S_5} \delta \mathbf{U}^T \mathbf{f} dS_5$$

$$= \rho \omega^2 h^2 \int_D \frac{1}{2} \delta \left( \mathbf{U}^T \mathbf{U} \right) dV - \int_D \left[ \frac{1}{2} \delta \left( \mathbf{E}^T \left( \mathbf{C} + \mathbf{S}^0 \right) \mathbf{E} \right) \right] dD - \int_{S_5} \delta \left( \mathbf{U}^T \mathbf{f} \right) dS_5$$

Consequently, we obtain

$$0 = \delta \left( \frac{1}{2} \int_D \left[ \rho \omega^2 h^2 \mathbf{U}^T \mathbf{U} - \mathbf{S}^T \left( [C] + \mathbf{\Sigma}^0 \right) \mathbf{S} \right] dD - \int_{S_5} \mathbf{U}^T \mathbf{f} dS_5 \right) \tag{12}$$

which is the variational form of the problem. From Equation (12), our problem can be organized as a total potential functional as follows:

$$\delta \left( \omega^2 \mathbf{K} - \mathbf{P} - \mathbf{M} \right) = 0 \tag{13}$$

where

$$\mathbf{K} = \frac{1}{2} \rho h^2 \int_D \mathbf{U}^T \mathbf{U} dD, \quad \mathbf{M} = \int_{S_5} \mathbf{U}^T \mathbf{f} dS_5, \text{ and } \mathbf{P} = \frac{1}{2} \int_D \left[ \mathbf{S}^T \left( [C] + \mathbf{\Sigma}^0 \right) \mathbf{S} \right] dD$$

Here, $\mathbf{K}$ is the kinetic energy, $\mathbf{P}$ is the potential energy, and $\mathbf{M}$ is the force energy, respectively.

For our solution procedure, we split the volume of the plate into the finite number of elements. Let $D_h$ be the volume of a brick element mesh, i.e., $D_h \subset D$, $D_{h_1} \cap D_{h_2} = \varnothing$, and $D = \bigcup D_h$. By the way, there are three degrees of freedom per element, i.e., $u_1$, $u_2$, and $u_3$. In particular, we consider the eight-noded isoparametric brick element. Figure 2 displays a geometrical configuration of a typical finite element. In this case, we can investigate the solution to problem in terms of the nodal displacements and their nodal virtual ones as follows:

$$\mathbf{U}^h = \mathbf{N} \mathbf{U}^{eh}, \quad \delta \mathbf{U}^h = \mathbf{N} \delta \mathbf{U}^{eh}, \quad \mathbf{U}^{eh} = \left[ u_{ui} \right]^T = \left[ u_{1i} \quad u_{2i} \quad u_{3i} \right]^T, \quad \mathbf{N} = \left[ N_1 \quad N_2 \quad \dots \quad N_8 \right] \text{ and } N_i = n_i I \quad (14)$$

where $u_{ui}$ is the nodal displacement components, $n_i$ is the linear basis function at the *i*th node, $I$ is the identity matrix, $\mathbf{N}$ is the shape function matrices of order $3 \times 24$, respectively. One can find the list of the shape functions in the monograph by Chandrupatla and Belegundu [37]. Further, the strain vector $\mathbf{E}^h$ can be written in term of the nodal displacement vector $\mathbf{U}^h$ as

$$\mathbf{S}^h = \mathbf{LNU}^{eh} = \mathbf{BU}^{eh} \tag{15}$$

$$\mathbf{B} = \left[ B_1 \quad B_2 \quad \dots \quad B_8 \right], \left[ B_i \right] = \begin{bmatrix} \dfrac{\partial n_i}{\partial x_1} & 0 & 0 & 0 & \dfrac{\partial n_i}{\partial x_3} & \dfrac{\partial n_i}{\partial x_2} \\ 0 & \dfrac{\partial n_i}{\partial x_2} & 0 & \dfrac{\partial n_i}{\partial x_3} & 0 & \dfrac{\partial n_i}{\partial x_1} \\ 0 & 0 & \dfrac{\partial n_i}{\partial x_3} & \dfrac{\partial n_i}{\partial x_2} & \dfrac{\partial n_i}{\partial x_1} & 0 \end{bmatrix}^T .$$

In order to obtain comfortably a solution to the problem, we can compute all the equations in the normalized coordinates $(r,s,t)$, instead of the local coordinates $\left(x_1^e, x_2^e, x_3^e\right)$. In this case, we can write

$$\mathbf{x}^e = \sum_{i=1}^{8} N_i\left(p,r,s\right)\mathbf{x}_i^e \ , \ \ \mathbf{x}^e = \begin{bmatrix} \mathbf{x}_1^e & \mathbf{x}_2^e & \mathbf{x}_3^e \end{bmatrix}^T, \text{ and } \mathbf{x}_i^e = \begin{bmatrix} \mathbf{x}_{i1}^e & \mathbf{x}_{i2}^e & \mathbf{x}_{i3}^e \end{bmatrix}^T$$

with the Jacobean matrix

$$\mathbf{J} = \begin{bmatrix} \sum_{i=1}^{8} \dfrac{\partial N_i}{\partial p}\mathbf{x}_{i1}^e & \sum_{i=1}^{8} \dfrac{\partial N_i}{\partial p}\mathbf{x}_{i2}^e & \sum_{i=1}^{8} \dfrac{\partial N_i}{\partial p}\mathbf{x}_{i3}^e \\ \sum_{i=1}^{8} \dfrac{\partial N_i}{\partial r}\mathbf{x}_{i1}^e & \sum_{i=1}^{8} \dfrac{\partial N_i}{\partial r}\mathbf{x}_{i2}^e & \sum_{i=1}^{8} \dfrac{\partial N_i}{\partial r}\mathbf{x}_{i3}^e \\ \sum_{i=1}^{8} \dfrac{\partial N_i}{\partial s}\mathbf{x}_{i1}^e & \sum_{i=1}^{8} \dfrac{\partial N_i}{\partial s}\mathbf{x}_{i2}^e & \sum_{i=1}^{8} \dfrac{\partial N_i}{\partial s}\mathbf{x}_{i3}^e \end{bmatrix} = \begin{bmatrix} \mathbf{D}_p\mathbf{x}_{i1}^e & \mathbf{D}_p\mathbf{x}_{i2}^e & \mathbf{D}_p\mathbf{x}_{i3}^e \\ \mathbf{D}_r\mathbf{x}_{i1}^e & \mathbf{D}_r\mathbf{x}_{i2}^e & \mathbf{D}_r\mathbf{x}_{i3}^e \\ \mathbf{D}_s\mathbf{x}_{i1}^e & \mathbf{D}_s\mathbf{x}_{i2}^e & \mathbf{D}_s\mathbf{x}_{i3}^e \end{bmatrix}, \ \mathbf{D}_v = \begin{bmatrix} \dfrac{\partial N_1}{\partial v} & \dfrac{\partial N_2}{\partial v} & \cdots & \dfrac{\partial N_8}{\partial v} \end{bmatrix}.$$
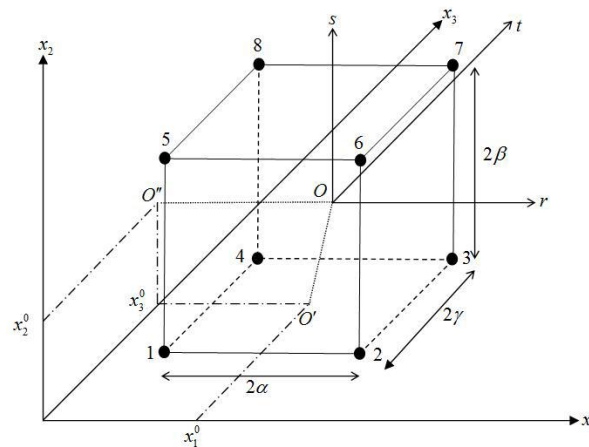


***Figure 2.** A typical finite element and the order of nodes*

Note that the determinant of the matrix $\mathbf{J}$ is positive every time due to the smooth shape of the finite element. We can, therefore, move the considered values from one coordinate system to other using the relation

$$\begin{bmatrix} \mathbf{D}_{x_1} & \mathbf{D}_{x_2} & \mathbf{D}_{x_3} \end{bmatrix}^T = \mathbf{J}^{-1}\begin{bmatrix} \mathbf{D}_p & \mathbf{D}_r & \mathbf{D}_s \end{bmatrix}^T.$$

With these explanations, we can re-write Equation (12) as follows:

$$\delta\left(\frac{1}{2}\int_{\tilde{D}}\left[\omega^2\left(\mathbf{U}^{eh}\right)^T\mathbf{M}^e\mathbf{U}^{eh} - \left(\mathbf{U}^{eh}\right)^T\mathbf{K}^e\mathbf{U}^{eh}\right]|\mathbf{J}|d\tilde{D} - \int_{S_5}\left(\mathbf{U}^{eh}\right)^T\mathbf{F}^e|\mathbf{J}|dS_5\right) = 0 \tag{16}$$

where

$$\mathbf{M}^e = \rho h^2\mathbf{N}^T\mathbf{N}, \ \mathbf{K}^e = \mathbf{B}^T\left(\mathbf{C}+\mathbf{S}^0\right)\mathbf{B}, \text{ and } \mathbf{F}^e = \mathbf{N}^T\mathbf{f}. \tag{17}$$

Here, $\mathbf{K}^e$ is the local stiffness matrix, $\mathbf{M}^e$ is the local mass matrix, and $\mathbf{F}^e$ is the local force vector. Further, if Equation (16) is re-organized according to the coefficients of $\mathbf{U}^{eh}$, we get the following system of equations:

$$\left(\mathbf{K}^e - \omega^2 \mathbf{M}^e\right)\mathbf{U}^{eh} = \mathbf{F}^e \tag{18}$$

where

$$\mathbf{K}^e = \int_{\tilde{D}} \mathbf{B}^T \left(\mathbf{C} + \mathbf{S}^0\right)\mathbf{B}|\mathbf{J}| d\tilde{D}, \ \mathbf{M}^e = \rho h^2 \int_{\tilde{D}} \mathbf{N}^T \mathbf{N}|\mathbf{J}| d\tilde{D}, \text{ and } \mathbf{F}^e = \int_{S_5} \mathbf{N}^T \mathbf{f}|\mathbf{J}| dS_5 . \tag{19}$$

As a result, we obtain the standard solution to the problem over the considered finite element. Using an appropriate transformation from local node number to global one, the local solution can be globalized as follows:

$$\left(\tilde{\mathbf{K}} - \omega^2 \tilde{\mathbf{M}}\right)\tilde{\mathbf{U}} = \tilde{\mathbf{F}} \tag{20}$$

where $\tilde{\mathbf{K}}$ and $\tilde{\mathbf{M}}$ are the global stiffness and mass matrices, $\tilde{\mathbf{U}}$ and $\tilde{\mathbf{F}}$ are the global displacement and force vector, respectively. When solving Equation (20), the values of the stress components over each node are obtained by employing Hook's relations.

## 4. NUMERICAL RESULTS

The dynamic response of the elastic three-dimensional plate based on a rigid foundation under a time-harmonic force is numerically discussed in this section. To this end, introduce the notations

$$\Omega = \omega h \sqrt{\frac{\rho}{\mu}}, \ \eta_{ij} = \frac{q_{ij}}{\mu}, \ a = \frac{a}{b}, \text{ and } \hat{h} = \frac{h_1}{2a} \tag{21}$$

where $\Omega$ is the dimensionless frequency parameter, $\eta$ is the initial stress parameter, $a$ is the aspect ratio, and $\hat{h}$ is the thickness ratio, respectively. To obtain general findings, we assume that $\Omega = 0$, $\eta = \eta_{11} = \eta_{33}$, $\eta = 0$, $a = 1$, $\hat{h} = 0.2$, and $v = 0.33$, where $v$ is the Poisson's ratio.

First of all, it is necessary to prove the convergence of the created algorithm. To do this, define the following relative error functions:

$$\|x\|_\infty = \max_i \|x_i\|_\infty , \ \|x\|_1 = \sum_i \|x_i\|_1 , \text{ and } \|x\|_0 = \sqrt{\sum_i \|x_i\|_0^2} .$$
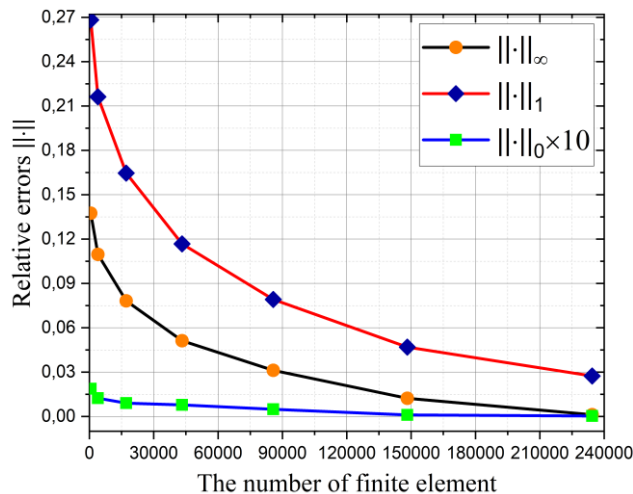


***Figure 3.*** *Distributions of error functions for various number of meshes*

Figure 3 provides a convergence analysis for our numerical results according to the above three norm functions. According to the general motivation of the finite element method, as the mesh number over the problem domain increases, the obtained numerical results must improve. The error graphs establish the predictions. It can be seen that as the number of finite elements increases, the errors converge to zero rapidly. In fact, it can be seen from the curves of the error functions that this convergence is quadratic. This means that even with a small increase in the number of finite elements, one can achieve higher accuracy. This indicates that the PC algorithm has been validated.
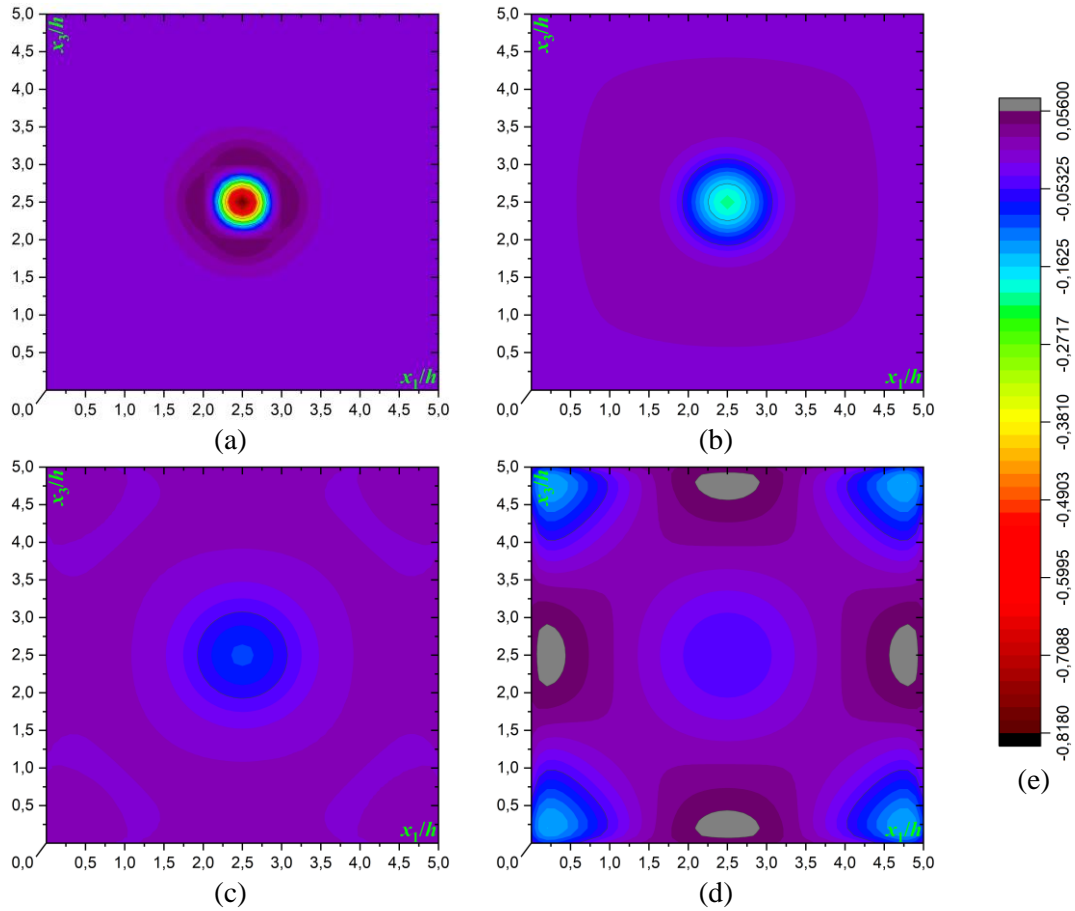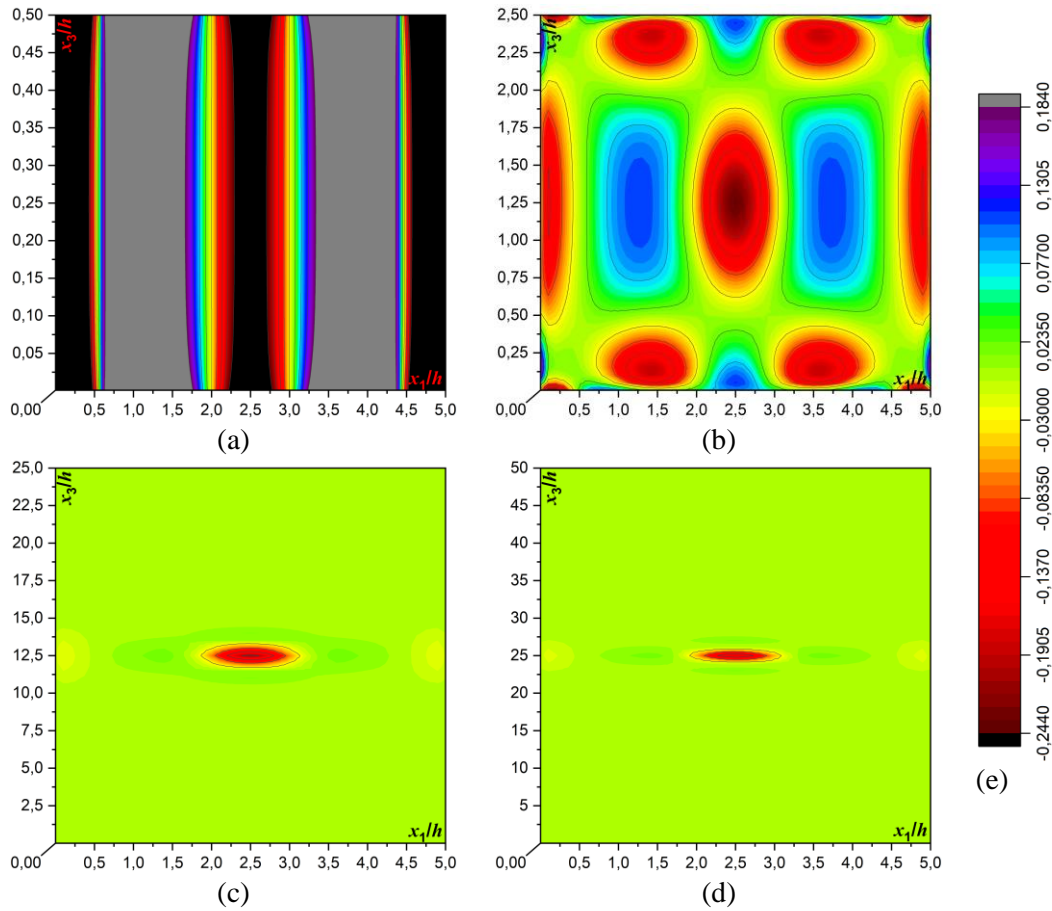


**Figure 4.** *Three-dimensional distributions of $\sigma_{22}h / p_0$ under (a) $\hbar = 0.1$, (b) $\hbar = 0.2$, (c) $\hbar = 0.3$, (d) $\hbar = 0.4$, and (e) Color scale*

Figure 4 supplies three-dimensional distributions of the stress $\sigma_{22}h / p_0$ on the plane $x_2 / h = -1$ for the cases where $\hbar = 0.1$ (Figure 4a), $\hbar = 0.2$ (Figure 4b), $\hbar = 0.3$ (Figure 4c), and $\hbar = 0.4$ (Figure 4d). It is seen that with increasing the ratio $\hbar$, the stress $\sigma_{22}h / p_0$ decrease. We conclude from the graphs that the stress distributions create three zones, namely, the reddish zone, the bluish zone, and the purplish zone. These may be called the main zone, the moderate zone, and the free zone, respectively. To be clear, these regions can be represented by

- $\left(x_1 / h - 2.5\right)^2 + \left(x_3 / h - 2.5\right)^2 < r_1^2$

- $r_1^2 < \left(x_1 / h - 2.5\right)^2 + \left(x_3 / h - 2.5\right)^2 < r_2^2$

- $r_2^2 < \left(x_1 / h - 2.5\right)^2 + \left(x_3 / h - 2.5\right)^2$.

In the main zone, the stress reaches relatively higher values. While the situation becomes calmed down in the moderate zone, the stress state vanishes almost in the free zone. These findings can be observed clearly from the color scale rod. In particular, for the case where $\hat{h} = 0.4$, the stress distribution is unstable and there are symmetric additional four. It is well-known from open literature that sometimes, there is a parametric resonance in the system for a specific value of the problem parameters. In this case, an unstable dynamic response of the system may be observed. This is indeed the case in Figure 4d. Additionally, it follows that the distribution of graph (b) coincides exactly with Figure 3.a of the paper in [35]. On the other hand, according to Equation (7), the stress values at the lateral sides of the plate converge to zero in the loss of the initial stress case. Taking the graphs into account, it follows that this speculation is valid, confirming the PC algorithm once again.



**Figure 5.** *Three-dimensional distributions of $\sigma_{22}h / p_0$ under (a) $a = 10$, (b) $a = 2$, (c) $a = 0.2$, (d) $a = 0.1$, and (e) Color scale*

Figure 5 provides the dynamic behavior of the normal stress $\sigma_{22}h / p_0$ on the plane $x_2 / h = -1$ for certain values of the aspect ratio $a$, i.e., $a = 10$ (Figure 5a), $a = 2$ (Figure 5b), $a = 0.2$ (Figure 5c), and $a = 0.1$ (Figure 5d). Here, the discussion will be held with Figure 4b ($\hat{h} = 0.2$ and $a = 1$) together. As the aspect ratio $a$ increases, $\sigma_{22}h / p_0$ decrease. For the case where $a = 1$, the stress distributions look like a circular shape, but in other cases, i.e., for $a \neq 1$, the distributions look like an ellipse shape. The main axis of the ellipse lies on the parallel line to the shorter side, at the center of the plane. According to the graphs, the main zone engages a certain area in each graph. But there is a strange case in Figure 5a. For certain values of $a *$ such that $a < a *$, the stress waves quickly hit the lateral sides of the plate because the size of the main zone covered by the stress waves is smaller than the surface of the plate. The regions where the stress takes relatively high values due to the impact occur on the side surfaces where the short edge is located. To be clear, the values of $a *$ can be detected from the graphs. The same comments can be made partially for Figure 5b.

Figure 6 displays the influence of the parameter $\eta$ on the dynamic reaction of $\sigma_{22}h/p_0$ on the plane $x_2/h = -1$, i.e., $\eta = -0.06$ (Figure 6a), $\eta = -0.03$ (Figure 6b), $\eta = 0.03$ (Figure 6c), and $\eta = 0.06$ (Figure 6d). It should be noted that we consider Figure 4b ($\hat{h} = 0.2$ and $\eta = 0$). By the way, these values are not random. The mechanical experiments in the literature prove that the initial stress values change over the range $-0.8 < \eta < 0.8$. Here, while the positive sign of $\eta$ denotes the initial stretching, the negative one implies the initial compressing. According to the graphs, an increase in the value of the initial compressing yields an increase in the stress value, but an increase in the value of the initial stretching leads to a decrease in the stress value in the medium. More precisely, the amplitude of the main zone decreases in accordance with the initial stress parameter $\eta$. However, the effect mentioned is somewhat limited. It is seen that the moderate and free zones are unaffected by the initial stress state.
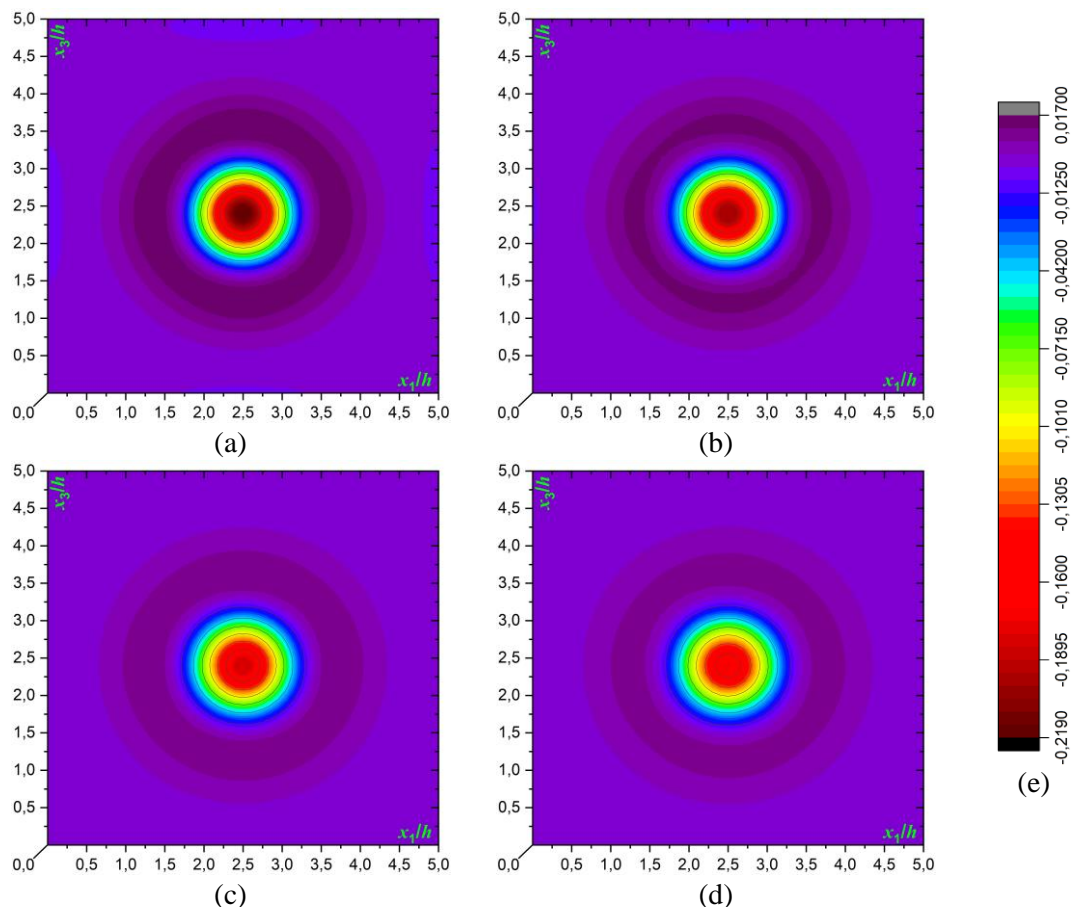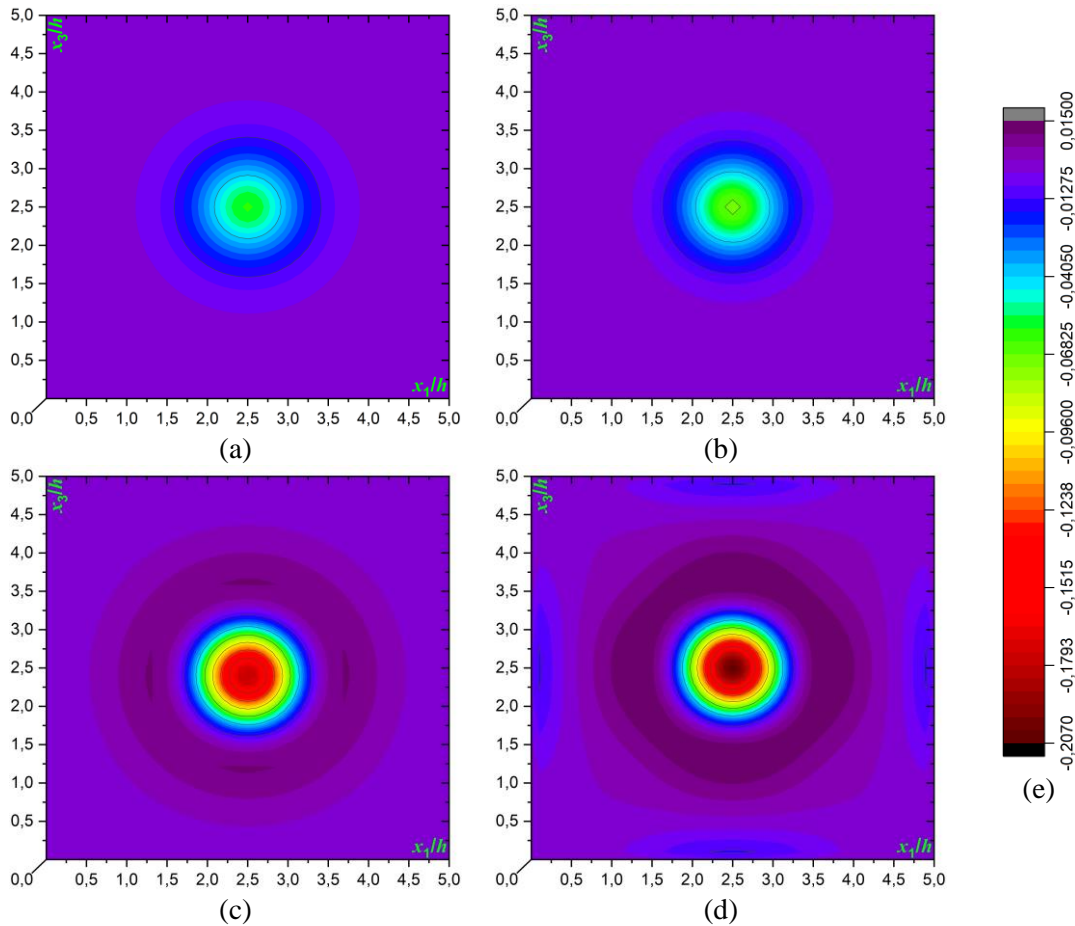


***Figure 6.*** *Three-dimensional distributions of $\sigma_{22}h/p_0$ under (a) $\eta = -0.06$, (b) $\eta = -0.03$, (c) $\eta = 0.03$, (d) $\eta = 0.06$, and (e) Color scale*

Figure 7 shows three-dimensional distributions of the stress $\sigma_{22}h/p_0$ on the plane $x_2/h = -1$ for certain values of the Poisson's ratio $\nu$, i.e., $\nu = 0.11$ (Figure 7a), $\nu = 0.22$ (Figure 7b), $\nu = 0.33$ (Figure 7c), and $\nu = 0.44$ (Figure 7d). The Poisson's ratio of linear, homogeneous, and isotropic materials changes over $-1.0 < \nu < 0.5$ since their Young's modulus, the shear modulus, and the bulk modulus must have positive values. It is established from the graphs that the absolute values of the normal stress $\sigma_{22}h/p_0$ decrease with the ratio $\nu$. Moreover, the main zone disappears with increasing the ratio $\nu$ and integrates immediately with the moderate zone. The results prove that the ratio $\nu$ is an important factor for the dynamical behavior of the plate in response to the external force.

Considering all the graphs in Figures 4 to 7, while there is a direct link between $\sigma_{22}h/p_0$ and $\hbar$, $a$ or $\nu$, there is an indirect link between $\sigma_{22}h/p_0$ and $\eta$. On the other hand, the stress $\sigma_{22}h/p_0$ reaches its unique maximal value at the middle point of the surface.

Above, we investigated three-dimensional graphs of the stress $\sigma_{22}h/p_0$ along the plate's bottom surface, but our primary purpose is to focus on the frequency response of the elastic plate under consideration. For this purpose, the next discussions will be carried out on the middle point of the bottom surface.



**Figure 7.** *Three-dimensional distributions of $\sigma_{22}h/p_0$ under (a) $\nu = 0.11$, (b) $\nu = 0.22$, (c) $\nu = 0.33$, (d) $\nu = 0.44$, and (e) Color scale*

Figure 8 provides some important results to explain the relationships between $\sigma_{22}h/p_0$ and $\Omega$ for particular values of the ratio $\hbar$. The absolute values of the stress $\sigma_{22}h/p_0$ increase with $\Omega$. To be clear, the dependency between $\sigma_{22}h/p_0$ and $\Omega$ is non-monotone. The graphs prove that there are some points where the stress $\sigma_{22}h/p_0$ has maximal values versus $\Omega$. Denote it by $\Omega^*$ and it is called the resonance value. An increase in the values of the thickness ratio $\hbar$ leads to a decrease in the values of $\Omega^*$. To be clear, the ratio $\hbar$ encourages the resonance mode of the plate. This means that the ratio $\hbar$ plays an important role in the dynamic reaction of the pre-stressed plate, not only in a quantitatively but also in a qualitatively. On the other hand, the number of local maximal values of the stress $\sigma_{22}h/p_0$ versus $\Omega$ increases with the ratio $\hbar$, too. From these results, one can say that the thickness ratio $\hbar$ increases the stability of the system. More precisely, a thicker plate means a more stable system.
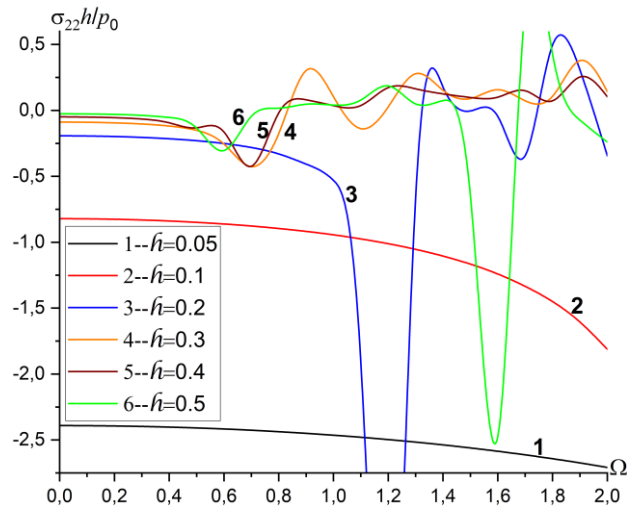
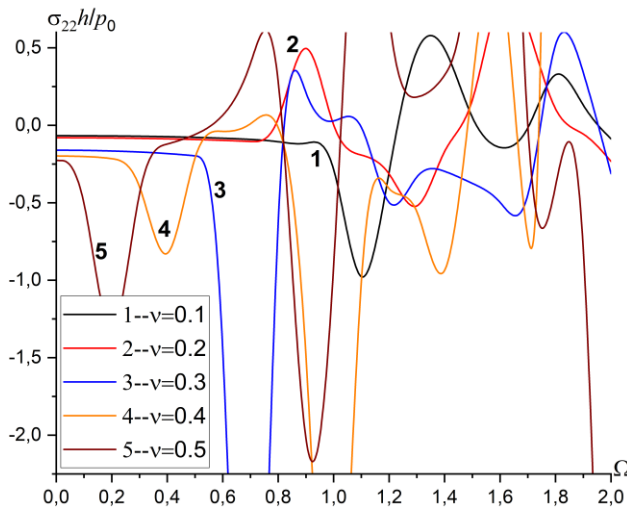**Figure 8.** *Dependency between $\sigma_{22}h/p_0$ and $\Omega$ for certain values of $\hbar$*



**Figure 9.** *Dependency between $\sigma_{22}h/p_0$ and $\Omega$ for certain values of $\nu$*
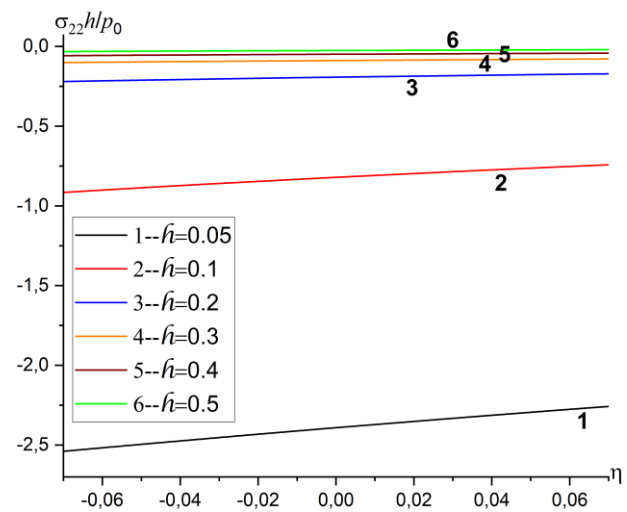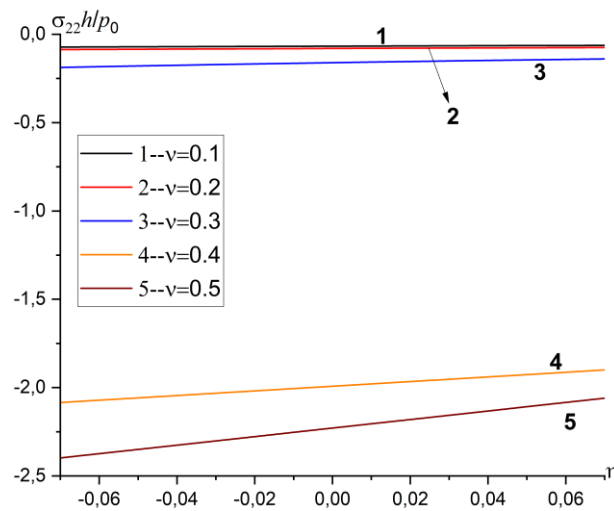


**Figure 10.** *Dependency between $\sigma_{22}h/p_0$ and $\eta$ for certain values of $\hbar$*

Figure 9 gives attention to the effect of the ratio $\nu$ on the frequency mode of the plate exposed to the time-harmonic force. It is shown from the graphs that the ratio $\nu$ has a serious effect on the mentioned response.

As the ratio $v$ increases, the values of $\Omega^*$ decrease. This means that the ratio $v$ exceeds that mode. Besides, the number of local maximal values of the stress $\sigma_{22}h/p_0$ increases as the ratio $v$ decreases. The influence of the ratio is important in the frequency response of the plate, qualitatively and quantitatively.

Figure 10 demonstrates the effect of the thickness ratio $\hat{h}$ on the relationship between $\sigma_{22}h/p_0$ and $\eta$. The graphs show that the mentioned dependency is linear. As in Figure 6, while the initial stretching parameter $\eta$ causes a decrease in the value of the stress $\sigma_{22}h/p_0$, the initial compressing parameter $\eta$ leads to, on the contrary, an increase. In consequence, the results are self-consistent, validating our algorithm again. The slopes of the graphs decrease as the ratio $\hat{h}$ increases. This means that the influence of the parameter $\eta$ on the dynamic response of the stress $\sigma_{22}h/p_0$ decreases as the ratio $\hat{h}$ increases. For the thinner plate, more efficiency is obtained from the initial stress in the medium.



***Figure 11.*** *Dependency between* $\sigma_{22}h/p_0$ *and* $\eta$ *for certain values of* $v$

Figure 11 presents the influence of the ratio $v$ on the relationship between $\sigma_{22}h/p_0$ and $\eta$. It follows from the graphs that the absolute values of the stress $\sigma_{22}h/p_0$ increase with the ratio $v$ and this effect is quite noticeable for $v > 0.3$. The slopes of the graphs decrease with the ratio $v$, in contrary to the one of the ratio $\hat{h}$. As a result, we conclude that increasing the ratio $v$ yields the influence of the parameter $\eta$ on the stress $\sigma_{22}h/p_0$ to increase.

## 5. CONCLUSIONS

The present problem is concerned with forced vibration analysis of a two-axially pre-loaded plate exposed to a time-harmonic force, covered by a rigid half-plane. A mathematical model is given according to the theory of linearized wave in elastic solids under a pre-loaded state (TLWESPS) and a solution procedure is proposed based on the three-dimensional finite element model. Some numerical results are discussed. Some of the inferences are summarized as follows:

- While increasing the thickness ratio causes to decrease the resonance values;
- The effect of initial stress parameter on the dynamic response of the plate increases with Poisson's ratio;
- Three stress zones occur at the bottom surface of the plate generally;
- An increase in the value of Poisson's ratio exceeds the resonance value of the plate;
- As the thickness ratio decreases, the effect of initial stress parameter on the dynamic response of the plate.

**CONFLICTS OF INTEREST**

No conflict of interest was declared by the authors.

**NOMENCLATURE**

| | | | |
|---|---|---|---|
| $a$ | Width of the plate | $\mathbf{P}$ | Potential energy |
| $\mathcal{a}$ | Aspect ratio | $q_{ij}$ | Pre-load parameter |
| $b$ | Depth of the plate | $S$ | Outward surfaces of the plate |
| $D$ | Volume of the plate | $\mathbf{S}$ | Stress vector |
| $E$ | Young's modulus | $t$ | Time parameter |
| $\mathbf{E}$ | Strain vector | $u_i$ | Displacement component |
| $\mathbf{F}^e$ | Local force vector | $\mathbf{U}^{eh}$ | Local displacement vector |
| $\tilde{\mathbf{F}}$ | Global force vector | $\mathbf{U}$ | Global displacement vector |
| $\mathbf{f}$ | Force vector | $\mathbf{V}$ | Virtual displacement function |
| $h$ | Height of the plate | $x_i$ | Cartesian coordinate component |
| $\hbar$ | Thickness ratio | $x_i'$ | Lagrangian coordinate component |
| $i$ | Complex unit | $\overline{x}_i$ | Normalized coordinate component |
| $\mathbf{J}$ | Jacobean matrix | $\mathbf{x}^e$ | Nodal coordinate vector |
| $\mathbf{K}$ | Kinetic energy | $\delta^*$ | Dirac's delta-function |
| $\mathbf{K}^e$ | Local stiffness matrix | $\varepsilon_{ij}$ | Strain component |
| $\tilde{\mathbf{K}}$ | Global stiffness matrix | $\eta_{ij}$ | Initial stress parameter |
| $\mathbf{L}$ | Gradient matrix | $\nu$ | Poisson's ratio |
| $\mathbf{M}$ | Force energy | $\rho$ | Mass density |
| $\mathbf{M}^e$ | Local mass matrix | $\sigma_{ij}$ | Stress component |
| $\tilde{\mathbf{M}}$ | Mass matrix | $\omega$ | Frequency of external force |
| $\mathbf{n}$ | Unit normalized vector | $\Omega$ | Dimensionless frequency parameter |
| $p_0$ | Value of the point-located force | | |

**REFERENCES**

[1] Barber, J. R., "Elasticity", Dordrecht: Kluwer Academic Publishers, (2002).

[2] Lurie, A. I., "Theory of Elasticity", Springer Science & Business Media, (2010).

[3] Southwell, R. V. V., "On the general theory of elastic stability", Philosophical Transactions of the Royal Society of London. Series A, Containing Papers of a Mathematical or Physical Character, 213(497-508): 187-244, (1914).

[4] Biezeno, C. B., and Hencky, H., "On the general theory of elastic stability", In: Proceedings Koninklijke Nederlandse Akademie van Wetenschappen, 31: 569-592, (1928).

[5] Biot, M. A., "XLIII. Non-linear theory of elasticity and the linearized case for a body under initial stress", The London, Edinburgh, and Dublin Philosophical Magazine and Journal of Science, 27(183): 468-489, (1939).

[6] Neuber, H., "Die Grundgleichungen der elastischen Stabilität in allgemeinen Koordinaten und ihre Integration", ZAMM-Journal of Applied Mathematics and Mechanics, 23(6): 321-330, (1943).

[7] Trefftz, E., "Zur theorie der stabilität des elastischen gleichgewichts", ZAMM-Journal of Applied Mathematics and Mechanics, 13(2): 160-165, (1933).

[8] Green, A. E., Rivlin, R. S., and Shield, R. T., "General theory of small elastic deformations superposed on finite elastic deformations", Proceedings of the Royal Society of London, Series A, Mathematical and Physical Sciences, 211(1104): 128-154, (1952).

[9] Guz, A. N., "Three-dimensional theory of elastic stability under finite subcritical deformations", Soviet Applied Mechanics, 8(12): 1308-1323, (1972).

[10] Zubov, L. M., "Theory of small deformations of prestressed thin shells: PMM", Journal of Applied Mathematics and Mechanics, 40(1): 73-82, (1976).

[11] Tiersten, H. F., "Perturbation theory for linear electroelastic equations for small fields superposed on a bias", The Journal of the Acoustical Society of America, 64(3): 832-837, (1978).

[12] Ogden, R. W., "Nonlinear Elastic Deformations", Ellis Horwood/Halsted Press, New York, (1984).

[13] Akbarov, S., and Guz, A. N., "Mechanics of Curved Composites (Vol. 78)", Springer Science & Business Media (2000).

[14] Reddy, J. N., "Mechanics of Laminated Composite Plates and Shells: Theory and Analysis", CRC press, (2003).

[15] Guz, A. N., "Fundamentals of the 3D Theory of Stability of Deformable Bodies", Springer, New York, (1999). [Translated from Russian by M. Kashtalian.]

[16] Akbarov, S. D., "Dynamics of Pre-strained Bi-material Elastic Systems: Linearized Three-dimensional Approach", Springer, (2015).

[17] Kepceler, T., "Torsional wave dispersion relations in a pre-stressed bi-material compounded cylinder with an imperfect interface", Applied Mathematical Modelling, 34(12): 4058-4073, (2010).

[18] Zamanov, A., and Agasiyev, E., "Dispersion of lamb waves in a three-layer plate made from compressible materials with finite initial deformations", Mechanics of Composite Materials, 46(6): 583-592, (2011).

[19] Eröz, M., "The stress field problem for a pre-stressed plate-strip with finite length under the action of arbitrary time-harmonic forces", Applied Mathematical Modelling, 36(11): 5283-5292, (2012).

[20] Akbarov, S. D., Hazar, E., and Eröz, M., "Forced vibration of the pre-stressed and imperfectly bonded bi-layered plate strip resting on a rigid foundation", Computers, Materials and Continua, 36(1): 23-48, (2013).

[21] Hu, W. T., Xia, T. D., and Chen, W. Y., "Influence of lateral initial pressure on axisymmetric wave propagation in hollow cylinder based on first power hypo-elastic model", Journal of Central South University, 21(2): 753-760, (2014).

[22] Ilhan, N., and Koc, N., "Influence of polled direction on the stress distribution in piezoelectric materials", Structural Engineering and Mechanics: An International Journal, 54(5): 955-971, (2015).

[23] Kurt, I., Akbarov, S. D., and Sezer, S., "Effect of uniaxial initial stresses, piezoelectricity and third order elastic constants on the near-surface waves in a stratified half-plane", Journal of Thermal Engineering, 3(4): 1346-1357, (2016).

[24]  Yeşil, U. B., "Forced and natural vibrations of an orthotropic pre-stressed rectangular plate with neighboring two cylindrical cavities", Computers, Materials and Continua, 53(1): 1-22, (2017).

[25]  Daşdemir, A., "A mathematical model for forced vibration of pre-stressed piezoelectric plate-strip resting on rigid foundation", MATEMATIKA: Malaysian Journal of Industrial and Applied Mathematics, 34(2): 419-431, (2018).

[26]  Daşdemir, A., "Dynamic response of a bi-axially pre-stressed bi-layered plate resting on a rigid foundation under a harmonic force", Proceedings of the Institution of Mechanical Engineers, Part C: Journal of Mechanical Engineering Science, 234(3): 784-795, (2020).

[27]  Selim, M. M., "Dispersion relation for transverse waves in pre-stressed irregular single-walled carbon nanotubes", Physica Scripta, 95(11): 115218, (2020).

[28]  Babych, S. Y., and Glukhov, Y. P., "On one dynamic problem for a multilayer half-space with initial stresses", International Applied Mechanics, 57(1): 43-52, (2021).

[29]  Mandi, A., Kundu, S., and Pal, P. C., "Surface wave scattering analysis in an initially stressed stratified media", Engineering Computations, 38(8): 3153-3173, (2021).

[30]  Bagirov, E. T., "On the influence of the inhomogeneous residual stresses on the dispersion of axisymmetric longitudinal waves in the hollow cylinder", Mechanics, 42(8): 25-35, (2022).

[31]  Kumawat, S., Praharaj, S., and Vishwakarma, S. K., "Dispersion of torsional surface waves in a threefold concentric compounded cylinder with imperfect interface", Waves in Random and Complex Media, 1-26, (2022).

[32]  Daşdemir, A., "Effect of interaction between polarization direction and inclined force on the dynamic stability of a pre-stressed piezoelectric plate", Mechanics Research Communications, 131: 104150, (2023).

[33]  Veliyev, Q. J., and Ipek, C., "The Influence of the Material Properties of an Inhomogeneous Pre-Stressed Hollow Cylinder Containing an Inviscid Fluid on the Dispersion of Quasi-Scholte Waves", International Applied Mechanics, 59(5): 619-629, (2023).

[34]  Dehghanian, Z., Fallah, F., and Farrahi, G. H., "Wave propagation analysis in pre-stressed incompressible hyperelastic multi-layered plates using a plate theory", European Journal of Mechanics-A/Solids 103: 105141, (2024).

[35]  Daşdemir, A., and Eröz, M., "Forced vibration of a bi-axially pre-stressed plate subjected to a harmonic point force and resting on a rigid foundation", Transactions of the Canadian Society for Mechanical Engineering, 43(3): 333-343, (2019).

[36]  Reddy, J. N., "Energy Principles and Variational Methods in Applied Mechanics", New York, John Wiley & Sons, (2017).

[37]  Chandrupatla, T., and Belegundu, A., "Introduction to Finite Elements in Engineering", Third Edition, Prentice Hall, Upper Saddle River, NJ, (2002).